

Comparison of single-nucleus and single-cell transcriptomes in hepatocellular carcinoma tissue

FEI WEN¹, XIAOJIE TANG¹, LIN XU² and HAIXIA QU²

¹School of Clinical Medicine, Qingdao University, Qingdao, Shandong 266000;

²Department of Gastroenterology, Qingdao Municipal Hospital, Shinan, Qingdao, Shandong 266071, P.R. China

Received May 20, 2022; Accepted August 17, 2022

DOI: 10.3892/mmr.2022.12855

Abstract. Single-nucleus RNA sequencing (snRNA-seq) is a method used to analyze gene expression in cells for which isolation is complex, such as those in hepatocellular carcinoma (HCC) tissues. It constitutes an alternative to single-cell RNA sequencing (scRNA-seq) by analyzing the nucleus rather than the whole cell; however, whether it can completely replace scRNA-seq in HCC remains to be clarified. In the present study, scRNA-seq was compared with snRNA-seq in tumor tissue obtained from patients with HCC, using the 10X Genomics Chromium platform. Seurat was also used to process the data and compare the differences between the two sequencing methods in identifying different cell types. In the present study, the transcriptomes of 14,349 single nuclei and 9,504 single cells were obtained from the aforementioned HCC tissue. A total of 21 discrete cell clusters, including hepatocytes, endothelial cells, fibroblasts, B cells, T cells, natural killer cells and macrophages were identified. Notably, a high number of hepatocytes were detected using snRNA-seq, while an increased number of immunocytes were identified in the tumor microenvironment using scRNA-seq. Results of the present study provided a comprehensive image of human HCC at a single-cell resolution. Moreover, results of the present study further demonstrated that snRNA-seq may be adequate in replacing scRNA-seq in certain cases, and snRNA-seq performs at an improved level in hepatocyte sequencing. Combined use of the two sequencing methods may contribute to the study of intercellular interactions.

Introduction

Advances in single-cell RNA sequencing (scRNA-seq) have revolutionized the ability to further investigate the transcriptional

status of individual cells. ScRNA-seq has been successfully applied to identify cell types and understand complex subsets in various cancers, including lung (1), breast (2) and colon cancer (3). By contrast, single cells are challenging to recover entirely from certain tissues, such as brain tissue (4), and certain single cells, such as adipocytes (5), are incompatible with the droplet-based single-cell approach. Furthermore, scRNA-seq is restricted to fresh tissues and cannot be used in frozen tissues.

Single-nucleus RNA-seq (snRNA-seq) provides a solution to the aforementioned issues, and has been used in pancreas, brain and archive tissues (6-8). SnRNA-seq may be applied to preserved or inseparable tissues, avoiding the need to separate cells into single-cell suspensions. It can preclude the potential changes in gene expression resulting from enzymatic cell separation methods (9,10). Previous studies have demonstrated a high degree of concordance in sensitivity and cell-type classification between snRNA-seq and scRNA-seq (1,11,12). In addition, snRNA-seq has been indicated to possess unique advantages in capturing long non-coding RNAs and precursor microRNAs in the nucleus (13). However, snRNA-seq exhibits a number of limitations. For example, Thrupp *et al* (14) demonstrated that a small number of genes enriched in microglial activation genes were missing from snRNA-seq data compared with scRNA-seq data in human microglia. This suggested that snRNA-seq is not suitable for detecting microglial activation in humans (14,15).

Hepatocellular carcinoma (HCC) is the fourth leading cause of cancer-related death worldwide (16). In 2015, there were 854,000 cases of liver cancer and 810,000 deaths worldwide (17). HCC often develops from liver fibrosis, making it difficult to isolate tumor cells. To date, the majority of single-cell sequencing studies in HCC have focused on nonparenchymal cells (18), such as immune cells. There are few studies based on hepatocytes and hepatocellular-nonparenchymal cell interactions (19,20).

The present study aimed to explore the differences between the two sequencing methods, to determine whether snRNA-seq can replace or complement scRNA-seq.

Materials and methods

Sample preparation. Tumor tissue samples obtained in March 2021 from a 65-year-old male patient with HCC who underwent curative resection at Qingdao Municipal Hospital (Qingdao, China) were used to perform scRNA-seq and snRNA-seq. The present study was approved (approval

Correspondence to: Professor Haixia Qu or Professor Lin Xu, Department of Gastroenterology, Qingdao Municipal Hospital, 5 Donghai Zhong Road, Shinan, Qingdao, Shandong 266071, P.R. China

E-mail: haixiaqu@126.com

E-mail: xulin1968@163.com

Key words: single-nucleus RNA sequencing, single-cell RNA sequencing, hepatocellular carcinoma

no. 2022003) by the ethics committee of Qingdao Municipal Hospital (Qingdao, China) and informed consent was obtained from the patient. Diagnosis was confirmed histologically.

For scRNA-seq, freshly excised tissue was rinsed with RPMI-1640 medium (Thermo Fisher Scientific, Inc.) and cut into 1-2-mm pieces. The samples were incubated at 37°C for 40 min with digestive solution, containing 0.25% trypsin (Thermo Fisher Scientific, Inc.) and 10 µg/ml DNase I (MilliporeSigma; Merck KGaA) dissolved in 5% FBS (Thermo Fisher Scientific, Inc.). Samples were manually oscillated every 5 min, and filtered twice using a 40-µm nylon mesh (Thermo Fisher Scientific, Inc.). Erythrocytes were removed using 1X Red Blood Cell Lysis Solution (Thermo Fisher Scientific, Inc.).

To ensure that each cell was paired with the beads in the gel bead emulsion, 10X library preparation, and sequencing beads with a unique molecular identifier (UMI) and cell barcode were loaded to a near saturation position. Polyadenylated RNA molecules were hybridized with microbeads after exposure to cell lysis buffers. The beads are recycled into a test tube for reverse transcription. During cDNA synthesis, the 5' end of each cDNA molecule identifies its cell of origin with the UMI and cell markers. In brief, 10X microbeads perform second strand cDNA synthesis, splicing and universal amplification. Sequencing libraries were prepared using randomly interrupted whole transcriptome amplifications to enrich the 3' ends of transcripts associated with cell barcodes and UMI.

For snRNA-seq, chopped liver tissue was resuspended in 0.5 ml cold Nuclei EZ lysis buffer (NUC-101; MilliporeSigma) and homogenized on ice with a Dounce grinder. The homogenates were sequentially filtered through 70- and 40-µm cell filters (Thermo Fisher Scientific, Inc.) and centrifuged at 4°C (speed, 1,000 × g) for 5 min to precipitate the nuclei. The precipitate was resuspended in 1 ml cold washing buffer (PBS containing 2% bovine serum albumin; MilliporeSigma) and subsequently filtered through a 20-µm cell filter (500 µm).

Sequencing on the 10X Chromium platform. The Chromium single cell 3' library was constructed using the Chromium single cell 3' library, gel beads, and multiple kits and chip kits (10X Genomics) according to the manufacturer's instructions. Cell suspensions with reverse transcription premixes and single cell 3'-gel beads were loaded onto a chrome single cell chip, with a single cell count of 2,000-8,000 per reaction. Samples were treated using a 10X Genomics V2 kit. After cell lysis, the first strand cDNA was synthesized and amplified according to the manufacturer's instructions. The amplification cycle was set to 12 cycles. The library was sequenced using Illumina HiSeq X Ten sequencing system and the human reference genome was mapped using CellRanger (10X Genomics) software (version 5.0.0, <https://www.10xgenomics.com/>).

Data analysis. Read demultiplexing and alignment to the GRCh38 human reference genome were performed using CellRanger. Additional conservative cut-off values were further applied based on the number of genes detected per cell (>200) and the percentage of mitochondrial UMI counts (<20%). Seurat (version 4.1.1, <https://satijalab.org/seurat/>) was used for further data processing and integration.

Anchors were identified using the FindIntegrationAnchors function with the default settings, which takes a list of Seurat objects as input. These anchors were used to integrate the two sets of data with the IntegrateData function.

Identification of highly variable genes was performed using Seurat and the MeanVarPlot function with the default settings to identify the top ~2,000 variable genes.

Cluster analysis was performed with Seurat using a graph-based clustering approach. Briefly, the JackStraw function with the default settings was used to determine significant principal components (P<0.0001), and these principal components were utilized to generate the k-nearest neighbours (KNN) graph based on the Euclidean distance in PCA (Principal component analysis) space. The edge weights between any two cells were refined based on the shared overlap in their local neighborhoods (Jaccard distance). Cells were subsequently clustered according to a smart local moving algorithm, which iteratively clusters cell groups together with the goal of optimizing the standard modularity function. The resolution for the FindClusters function was set to 0.5. High modularity networks possess dense connections between the nodes within a given module, and sparse connections between nodes in different modules. Clusters were visualized using a uniform manifold approximation and projection for dimension reduction (UMAP) plot.

Differential expression analysis was performed in Seurat utilizing the FindAllMarkers function with the default settings.

Gene Ontology (GO) annotations were analyzed using clusterProfiler (version 4.2.2, <https://bioconductor.org/packages/release/bioc/html/clusterProfiler.html>). Adjusted P<0.05 was considered to indicate a statistically significant difference. The barplot function was used in clusterProfiler for graphical visualization.

Monocle2 (version 2.22.0, <http://cole-trapnell-lab.github.io/monocle-release/docs/>) (21) algorithm was used to analyze the differentiation status of hepatocytes. The orderCells function was used to sort and visualize cells arranged along a quasi-chronological trajectory. Using the differentialGeneTest function, the differentially expressed genes were calculated and visualized.

The CellphoneDB (version 3.0.0, <https://pypi.org/project/CellPhoneDB/>) (22) algorithm was used to obtain receptor-ligand pairs to analyze the interaction between HCC cells and T cells. Extracted normalized count data from the Seurat object were used as input.

All UMAP plots, violin plots and heatmaps in the present study were generated using Seurat functions combined with the ggplot2 and pheatmap R packages (version 4.1.2).

Results

RNA-seq profiling and comparison of transcriptomes between single nuclei and single cells. In total, 14,349 single nuclei and 9,504 single cells were isolated from the same HCC sample and sequencing was performed. The integration and clustering results are presented in Fig. 1. Notably, 97.1% single nuclei and 97.9% single cells passed quality control (Table I). SnRNA-seq matched an increased number of genes (nFeature, 2,933 vs. 1,297) than scRNA-seq. Moreover, scRNA-seq detected a higher number of counts (nCount, 42,940 vs. 25,070) than snRNA-seq

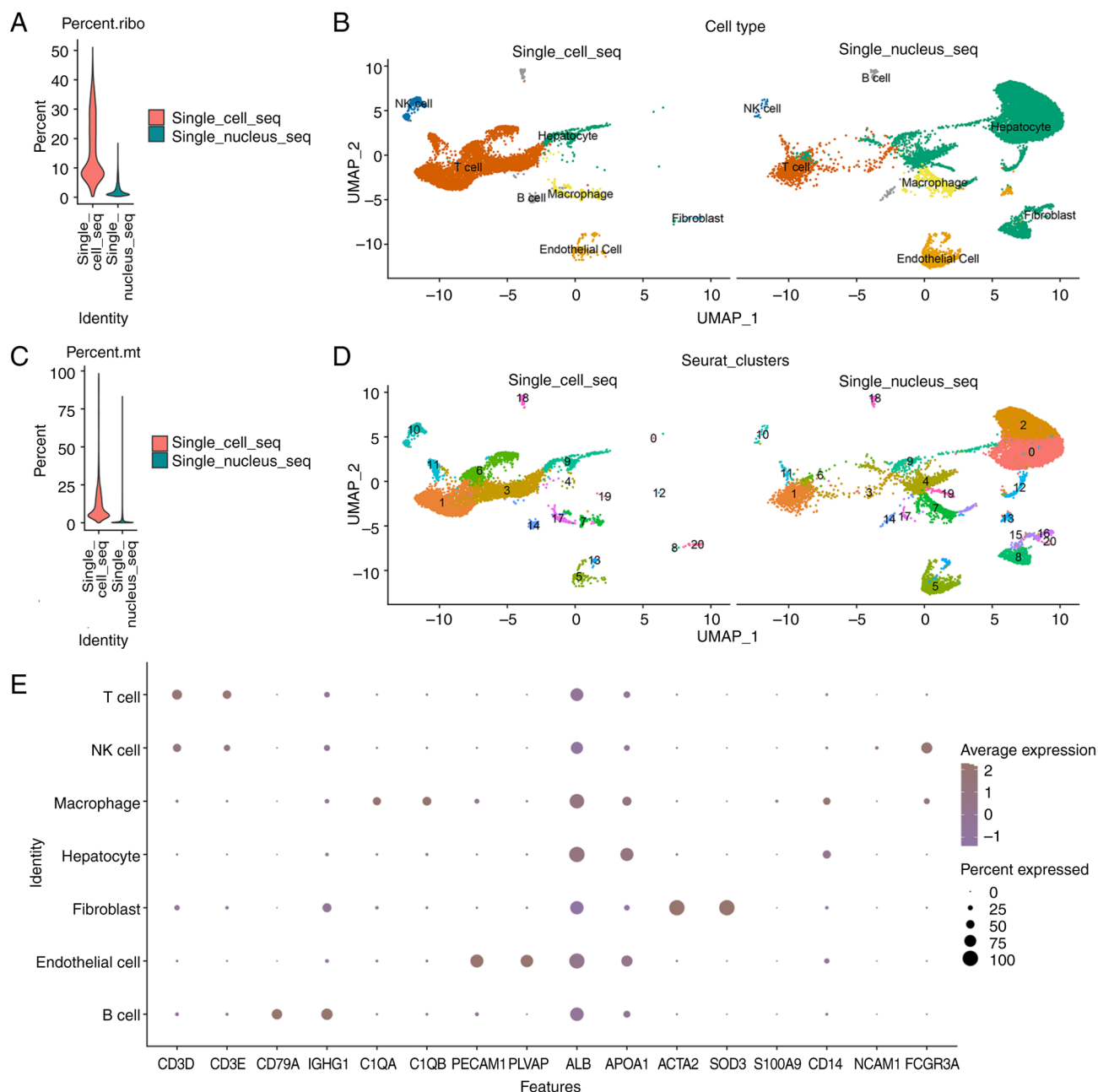


Figure 1. Integrated scRNA-seq and snRNA-seq datasets in HCC to identify and characterize cell types. (A) Violin plot of the ribosome proportion of two sequencing methods. (B) Uniform Manifold Approximation and Projection visualization of 14,349 single nuclei and 9,504 single cells from the same HCC sample. Clustering was divided into 7 main cell types. (C) Violin plot of the mitochondrial proportion of two sequencing methods. (D) Clustering was divided into 21 clusters. (E) Dotplot of marker genes expressed in T cells (CD3D and CD3E), macrophages/monocytes (C1QA and C1QB), B cells (CD79A and IGHG1), NK cells (NCAM1 and FCGR3A), endothelial cells (PECAM1 and PLVAP), hepatocytes (ALB and APOA1) and fibroblasts (SOD3 and ACTA2). snRNA-seq, single-nucleus RNA sequencing; scRNA-seq, single-cell RNA sequencing; HCC, hepatocellular carcinoma.

(Table I). Ribosome- and mitochondria-associated genes were identified at a higher rate using scRNA-seq than by using snRNA-seq (Fig. 1A and C), suggesting that the sample digestion step prior to scRNA-seq exerts an influence on cell activity, and snRNA-seq may maintain cell activity at an improved rate.

Cell types identified with nuclei and cells. A total of 21 clusters were identified in the integrated data and were matched to seven cell types, according to the expression levels of marker genes (Fig. 1B, D and E). There were four types of immune cells: T cells (n, 6,903; represented by the marker genes CD3D and CD3E), macrophages/monocytes (n, 950; C1QA and

C1QB), B cells (n, 426; CD79A and IGHG1) and natural killer (NK) cells (n, 453; NCAM1 and FCGR3A). A total of three types of nonimmune cells were identified: Endothelial cells (n, 1,361; PECAM1 and PLVAP), hepatocytes [n, 9,999; ALB and apolipoprotein (APO)A1] and fibroblasts (n, 61; SOD3 and ACTA2). The expression of marker genes in each cluster is displayed in Fig. 1B. The cell number/proportion of each cluster is displayed in the supplementary files (Tables SI and SII).

The cell types and cell numbers identified by snRNA-seq and scRNA-seq were compared and the results are provided in Figs. 2 and 3. An increased number of hepatocytes and endothelial cells were detected using snRNA-seq, and an increased

Table I. Quality control indicators from the Cell Ranger analysis.

Quality control indicator	snRNA-seq	scRNA-seq
Valid Barcodes, %	97.1	97.9
Valid UMIs, %	99.9	100.0
Reads Mapped Confidently to Intronic Regions, %	44.7	15.2
Mean Reads per Cell, n	25,070	42,940
Median Genes per Cell, n	2,933	1,297

UMI, unique molecular identifier; snRNA-seq, single-nucleus RNA sequencing; scRNA-seq, single-cell RNA sequencing.

Table II. Number of counts of each cell type using different sequencing methods.

A, Single_cell_seq	
Cell type	nCount_RNA (mean)
B cell	5,615.354
Endothelial cell	7,232.253
Fibroblast	8,661.491
Hepatocyte	4,634.638
Macrophage	5,799.175
NK cell	3,581.912
T cell	3,121.749

B, Single_nucleus_seq

Cell type	nCount_RNA (mean)
B cell	1,861.378
Endothelial cell	4,152.666
Fibroblast	12,047.000
Hepatocyte	7,479.514
Macrophage	2,213.186
NK cell	1,509.762
T cell	1,524.906

Seq, sequencing; NK, natural killer.

number of T cells, B cells and NK cells were detected using scRNA-seq (Fig. 2A and B). Moreover, ~95% of the hepatocytes and 87% of the endothelial cells were obtained from the snRNA-seq data, and 82% of the T cells, 77% of the B cells and 95% of the NK cells were obtained from the scRNA-seq data. By comparison, the snRNA-seq data was mainly composed of hepatocytes and endothelial cells, accounting for 75 and 9% of the cells, respectively. The scRNA-seq data was mainly composed of T cells, B cells, macrophages and NK cells, accounting for 75.5, 4, 5 and 5% of the cells, respectively (Fig. 2C).

Table III. Number of genes in each cell type using different sequencing methods.

A, Single_cell_seq	
Cell type	nFeature_RNA (mean)
B cell	1,338.933
Endothelial cell	2,511.374
Fibroblast	2,621.561
Hepatocyte	1,089.046
Macrophage	1,618.307
NK cell	1,336.354
T cell	1,061.945

B, Single_nucleus_seq

Cell type	nFeature_RNA (mean)
B cell	1,154.816
Endothelial cell	2,160.562
Fibroblast	4,219.500
Hepatocyte	3,361.830
Macrophage	1,248.745
NK cell	1,056.952
T cell	1,015.813

Seq, sequencing; NK, natural killer.

SnRNA-seq identified a higher number of genes (nCount and nFeature) in hepatocytes and fibroblasts (Tables II and III; Fig. 2F and G). In the hepatocyte population, 1,089.046 genes (mean nFeature) were identified using scRNA-seq, and 3,361.830 genes were identified using snRNAseq (4,634.638 vs. 7,479.514 mean nCount). In the fibroblast subpopulation, 2,621.561 genes were identified using scRNA-seq, and 4,219.500 genes were identified using snRNAseq (8,661.491 vs. 12,047.000 mean nCount). Notably, other cell type clusters demonstrated a different trend. For example, in the T cell subpopulation, 1,061.945 genes were identified using scRNA-seq, and 1,015.813 genes were identified using snRNAseq (3,121.749 vs. 1,524.906 mean nCount).

Hepatocyte cluster analysis. A total of 9,999 hepatocytes were obtained, composing of clusters 0, 2, 4, 8, 9, 12, 15, 16 and 19. Overall, the snRNA-seq data contained the majority of cells (n=9,563) in the hepatocyte clusters, while the scRNA-seq data contained only part of the hepatocytes (n=436) in cluster 9 (Fig. 2D and E; Fig. 3A; Table SI).

Results presented in Fig. 4A demonstrated the differentially expressed genes in the hepatocyte clusters, and the top 20 genes are displayed in the heatmap. GO enrichment (biological process) results presented in Fig. 4B-J demonstrated the differentially expressed genes in the hepatocyte clusters. By combining the differential gene expression and GO enrichment analysis results, the function of each hepatocyte was analyzed in the subpopulation.

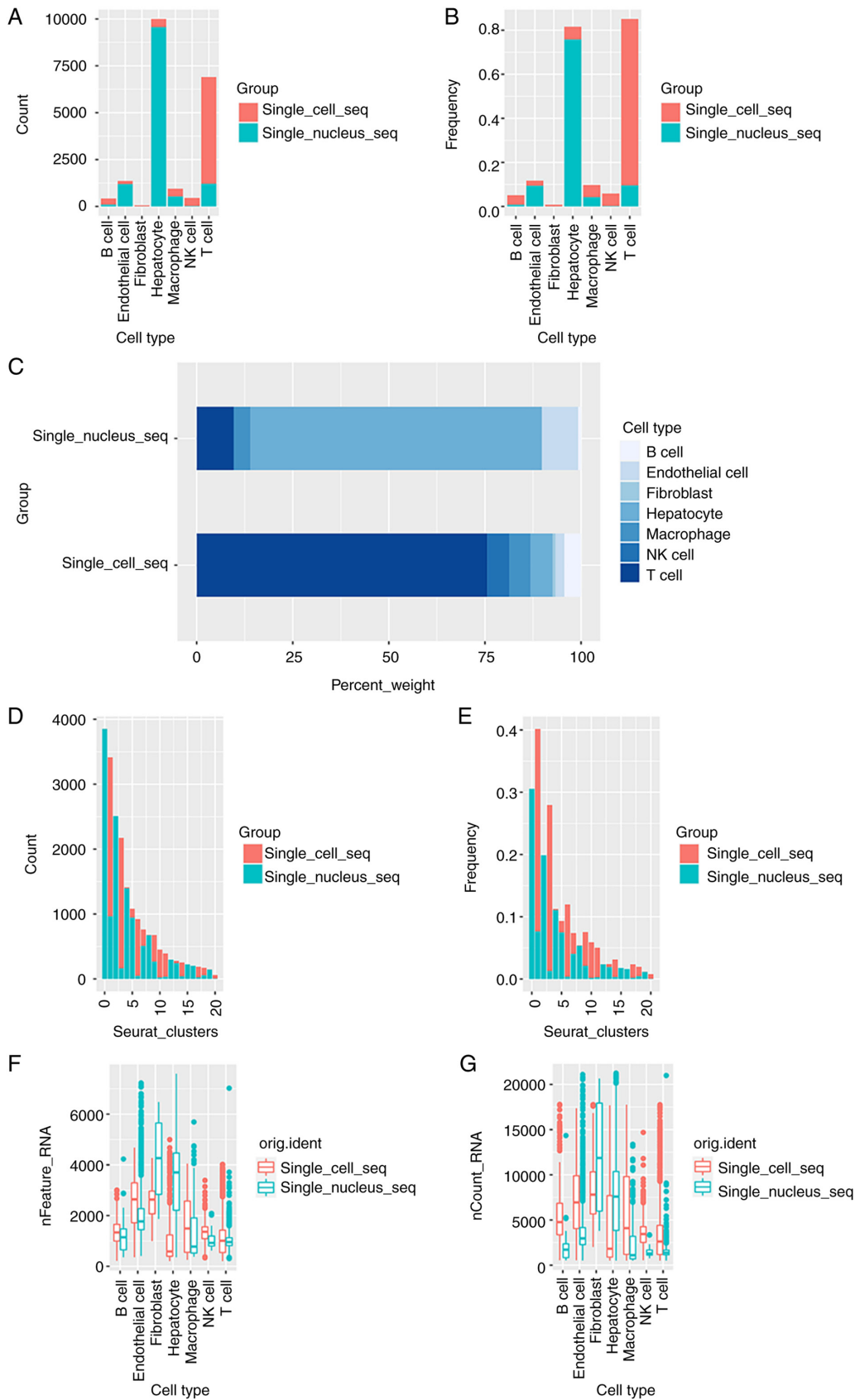


Figure 2. Comparison of cell types and cell numbers identified using scRNA-seq and snRNA-seq. (A) Barplot of numbers of T cells, macrophages/monocytes, B cells, NK cells, endothelial cells, hepatocytes and fibroblasts identified using scRNA-seq and snRNA-seq. (B) Barplot of proportions of T cells, macrophages/monocytes, B cells, NK cells, endothelial cells, hepatocytes and fibroblasts identified using scRNA-seq and snRNA-seq. (C) Barplot of cell compositions identified using scRNA-seq and snRNA-seq. (D) Barplot of numbers of 0-20 clusters identified using scRNA-seq and snRNA-seq. (E) Barplot of proportions of 0-20 clusters identified using scRNA-seq and snRNA-seq. (F) Barplot of nFeatures of T cells, macrophages/monocytes, B cells, NK cells, endothelial cells, hepatocytes and fibroblasts identified using scRNA-seq and snRNA-seq. (G) Barplot of nCount of T cells, macrophages/monocytes, B cells, NK cells, endothelial cells, hepatocytes and fibroblasts identified using scRNA-seq and snRNA-seq. snRNA-seq, single-nucleus RNA sequencing; scRNA-seq, single-cell RNA sequencing; NK, natural killer.

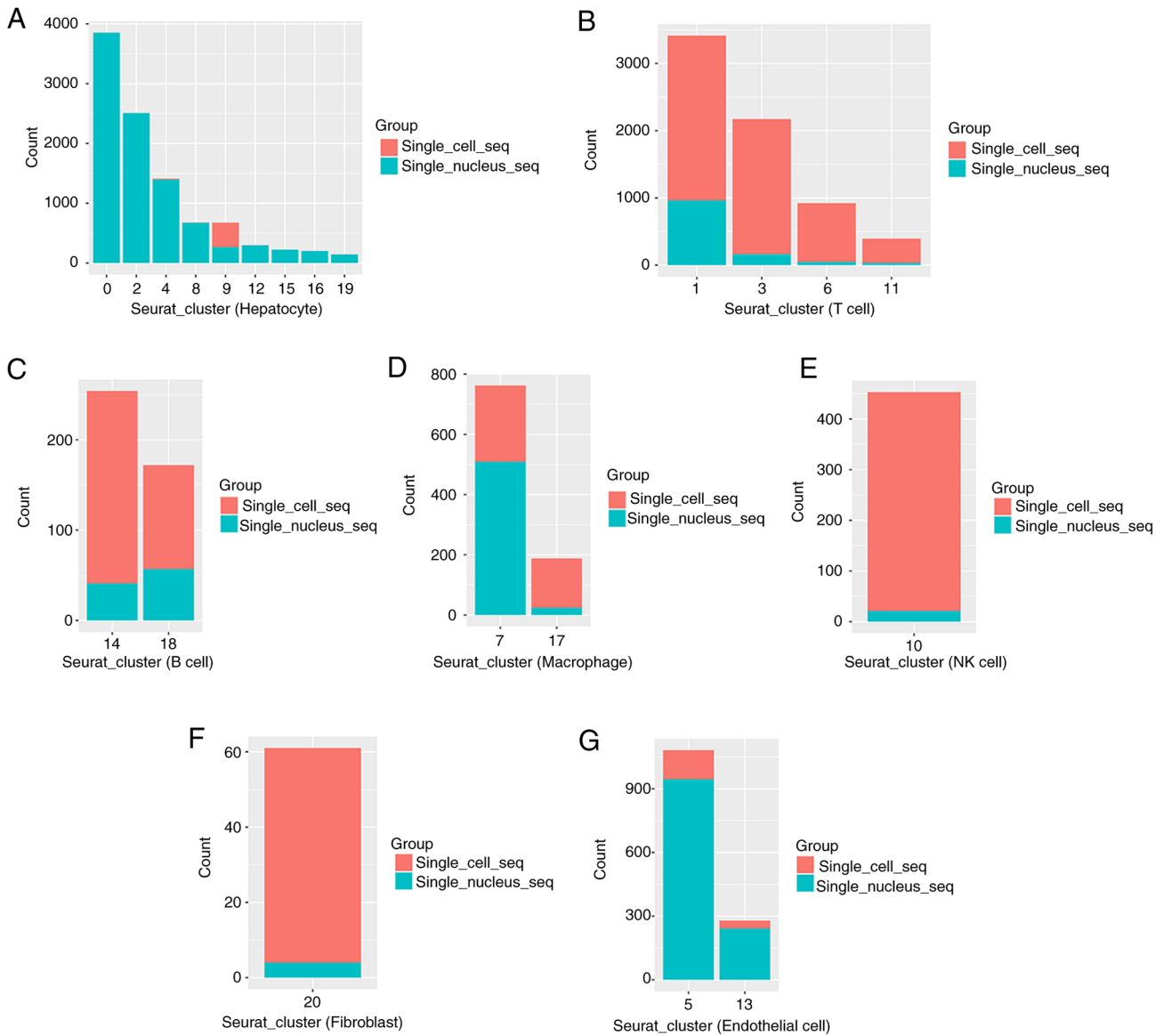


Figure 3. Comparison of numbers of subclusters in each cell type between scRNA-seq and snRNA-seq. (A) Barplot of numbers of subclusters in hepatocytes identified using scRNA-seq and snRNA-seq. (B) Barplot of numbers of subclusters in T cells identified using scRNA-seq and snRNA-seq. (C) Barplot of numbers of subclusters in B cells identified using scRNA-seq and snRNA-seq. (D) Barplot of numbers of subclusters in macrophages/monocytes identified using scRNA-seq and snRNA-seq. (E) Barplot of numbers of subclusters in NK cells identified using scRNA-seq and snRNA-seq. (F) Barplot of numbers of subclusters in fibroblasts identified using scRNA-seq and snRNA-seq. (G) Barplot of numbers of subclusters in endothelial cells identified using scRNA-seq and snRNA-seq. snRNA-seq, single-nucleus RNA sequencing; scRNA-seq, single-cell RNA sequencing; NK, natural killer.

Cluster 0 exhibited differential expression of *CYP3A5*, *MLIP* and *ESR1*, and ‘regulation of lipid metabolic process’ and ‘triglyceride metabolic process’ were identified as the enriched terms in GO analysis (Fig. 4B). Cluster 2 exhibited high expression of *ATF5*, *GPAM* and *FGF12*, and the enriched terms were mainly associated with ‘negative regulation of hydrolase activity’ and ‘blood coagulation, fibroclot formation’ (Fig. 4C). Cluster 4 was marked by *APOA2* and *APOC1*, and ‘regulation of lipid catabolic process’ was enriched (Fig. 4D). Cluster 8 exhibited high expression of extracellular matrix-related proteins, such as *PRKG1*, *RBMS3* and *ITGBL1*, suggesting a function in matrix remodeling and cell migration (Fig. 4E). Cluster 9 exhibited differential expression of *MT-ND2*, *MT-ND4* and *MT-ND1*, and ‘negative regulation of blood coagulation’ and ‘negative regulation of haemostasis’ were identified as the enriched terms in GO

analysis (Fig. 4F). Cluster 12 was marked by *ASPM*, *DIAPH3* and *BRIP1*, and cell proliferation-related pathways, including ‘mitotic nuclear division’ and ‘mitotic sister chromatid segregation’ were enriched (Fig. 4G).

To analyze the temporal dynamics of hepatocyte differentiation, single cells were rearranged into a pseudo-timeline using Monocle2, and the results of the analysis are presented in Fig. 5. Results of the present study demonstrated the differentiation status of hepatocytes (Fig. 5A), and the distribution of different clusters was concentrated (Fig. 5C). The differential expression of cells in different states of differentiation were analyzed, and genes with increased expression levels are demonstrated in heatmaps (Fig. 5B).

In summary, snRNA-seq retained multiple heterogeneous hepatocyte subpopulations, whereas scRNA-seq only retained

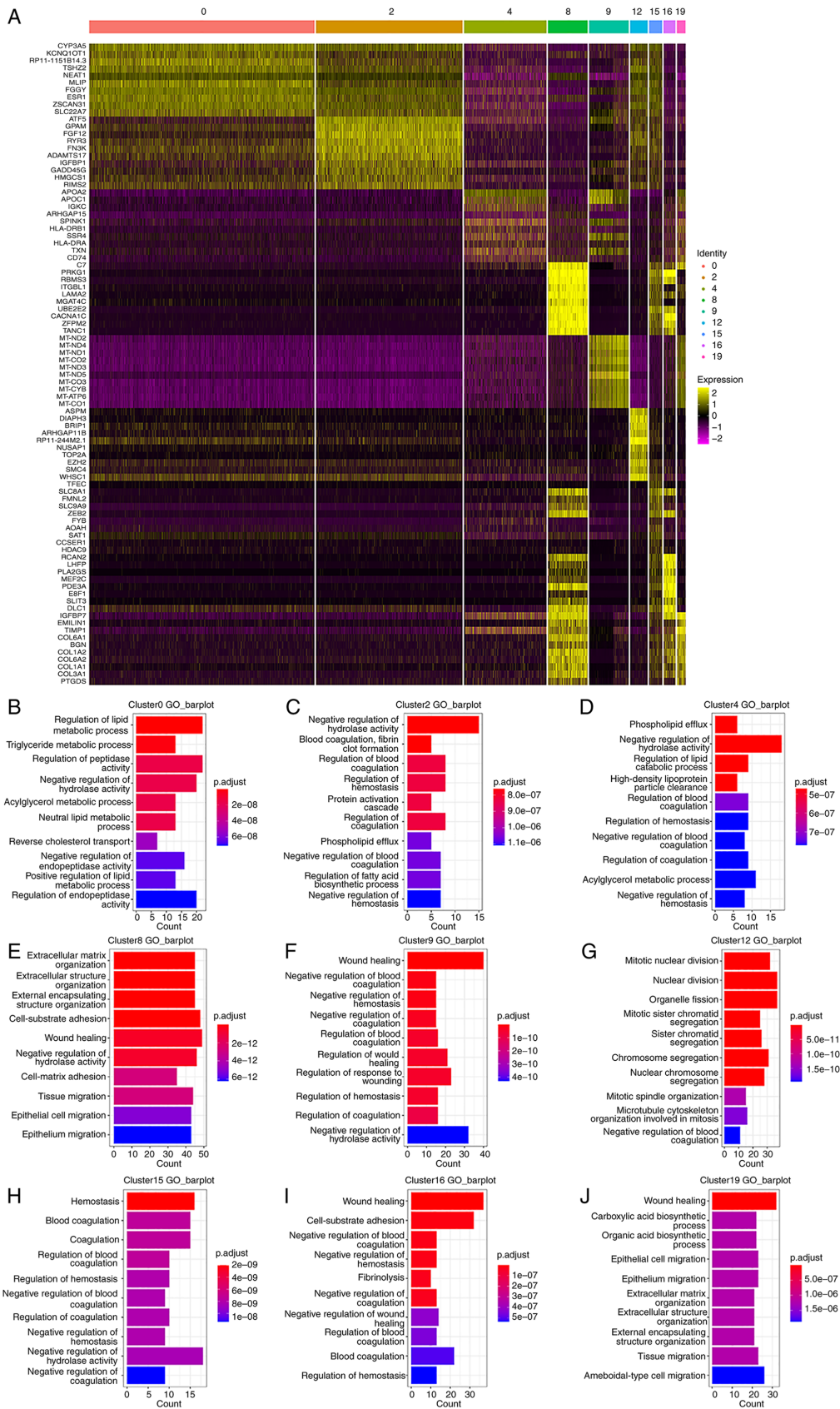


Figure 4. Subgroup analysis of hepatocytes. (A) Heatmap of the top 20 differentially expressed genes in hepatocyte clusters (cluster 0, 2, 4, 8, 9, 12, 15, 16, 19). (B) GO enrichment (biological process) results of differentially expressed genes in hepatocyte cluster 0. (C) GO enrichment (biological process) results of differentially expressed genes in hepatocyte cluster 2. (D) GO enrichment (biological process) results of differentially expressed genes in hepatocyte cluster 4. (E) GO enrichment (biological process) results of differentially expressed genes in hepatocyte cluster 8. (F) GO enrichment (biological process) results of differentially expressed genes in hepatocyte cluster 9. (G) GO enrichment (biological process) results of differentially expressed genes in hepatocyte cluster 12. (H) GO enrichment (biological process) results of differentially expressed genes in hepatocyte cluster 15. (I) GO enrichment (biological process) results of differentially expressed genes in hepatocyte cluster 16. (J) GO enrichment (biological process) results of differentially expressed genes in hepatocyte cluster 19. GO, Gene Ontology.

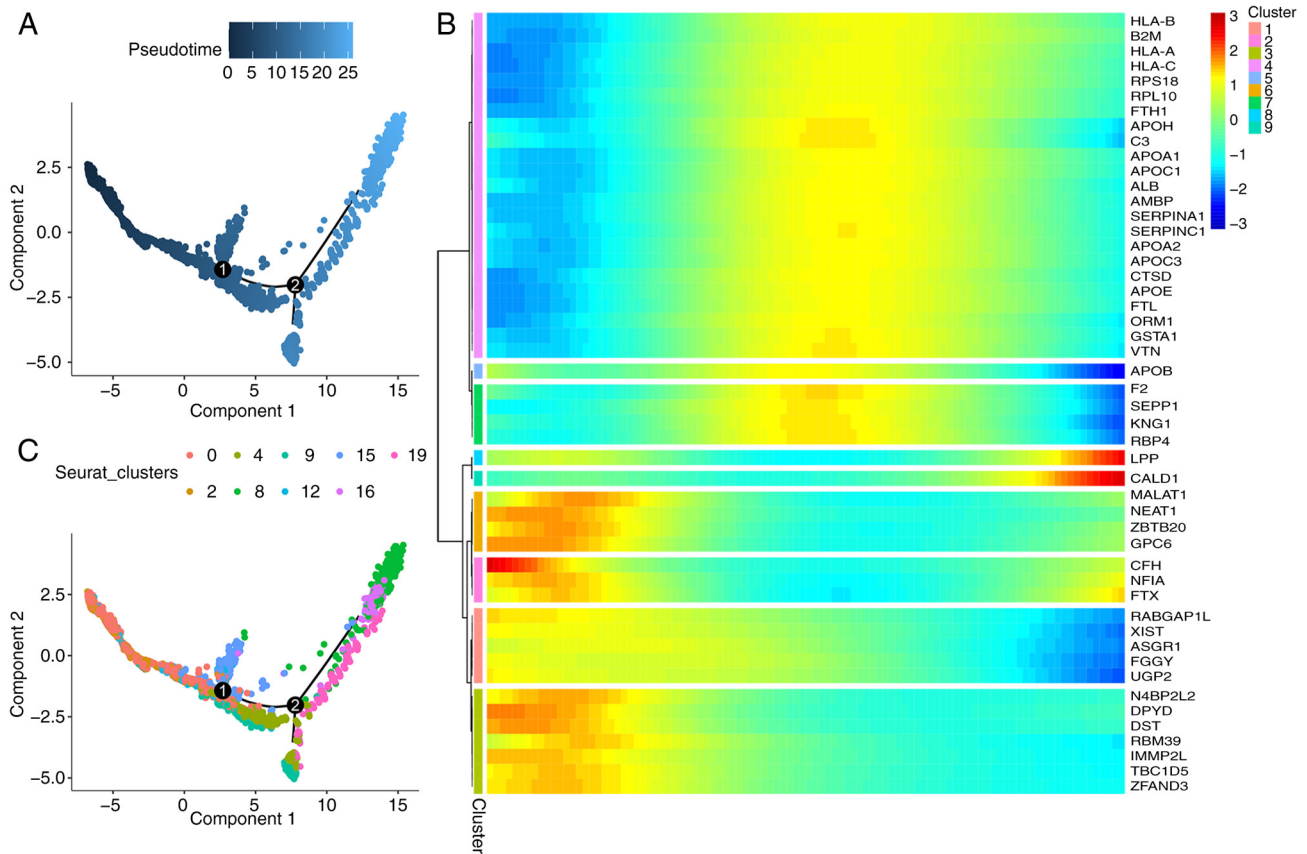


Figure 5. Pseudotime analysis of hepatocyte subclusters. (A) Plot of trajectory colored with pseudotime. (B) Plot of trajectory colored with subclusters (cluster 0, 2, 4, 8, 9, 12, 15, 16, 19). (C) Pseudotime heatmap of differentially expressed genes (with high expression levels).

a single subpopulation (Cluster 9), suggesting that this subpopulation may be insensitive to the digestion step prior to scRNA-seq and is easy to retain. SnRNA-seq possesses notable advantages in maintaining the heterogeneity of tumor cells in HCC tissues.

T cell cluster analysis. T cells were the largest subset of immune cells, and there were significant differences between the two sequencing methods; thus, a detailed analysis was conducted.

A total of 6,904 T cells were obtained, including clusters 1, 3, 6 and 11. The scRNA-seq data contained most of the cells in clusters 1, 3, 6 and 11, while the snRNA-seq data only contained part of the Cluster 1 cells (Figs. 2D and E and 3B).

The results displayed in Fig. 6A demonstrate the differentially expressed genes in the T cell clusters, and the top 20 genes are displayed in the heatmap. Fig. 6B demonstrates the marker genes of the four T cell clusters. Fig. 6C-F demonstrates the GO enrichment (biological process) results for the differentially expressed genes in the T cell clusters. By combining the differential gene expression and GO enrichment analysis results, the function of each T cell cluster was analyzed.

Cluster 1 exhibited differential expression of INPP4B, THEMIS and CCR7, and ‘regulation of humoral immune response’ was identified as the enriched term in the GO analysis (Fig. 6C); thus, these cells were classified as naive

CD4⁺ T cells. Cluster 3 exhibited differential expression of mitochondrially encoded MT-ND1, MT-ND2 and MT-ND4, and ‘negative regulation of blood coagulation’ was identified as the enriched term in the GO analysis (Fig. 6D). Cluster 6 exhibited differential expression of TPX2, EZH2, GZMB and ‘mitotic sister chromatid segregation’ and ‘sister chromatid segregation’ were identified as the enriched terms in the GO analysis; thus, these cells were classified as effector CD8⁺ T cells (Fig. 6E). Cluster 11 exhibited the differential expression of CTLA4, DLGAP1 and TNFRSF18, and ‘negative regulation of endopeptidase activity’ and ‘negative regulation of peptidase activity’ were identified as the enriched terms in the GO analysis (Fig. 6F); thus, these cells were classified as depleted CD8⁺ T cells. Overall, these results indicated that cluster 1 is associated with immune regulation, cluster 3 is associated with coagulation, cluster 6 is associated with cell division and cluster 11 is associated with regulation of enzyme activity.

By comparison, results of the present study demonstrated that scRNA-seq retains multiple heterogeneous T cell subsets, while snRNA-seq retains only a single subset (cluster 1). These results suggested that scRNA-seq exhibits notable advantages in maintaining the heterogeneity of immune cells, particularly T cells.

The interaction between hepatocytes and T cells (ligand-receptor interactions). T cells primarily act as tumor-infiltrating lymphocytes, and their interactions with tumor cells have received

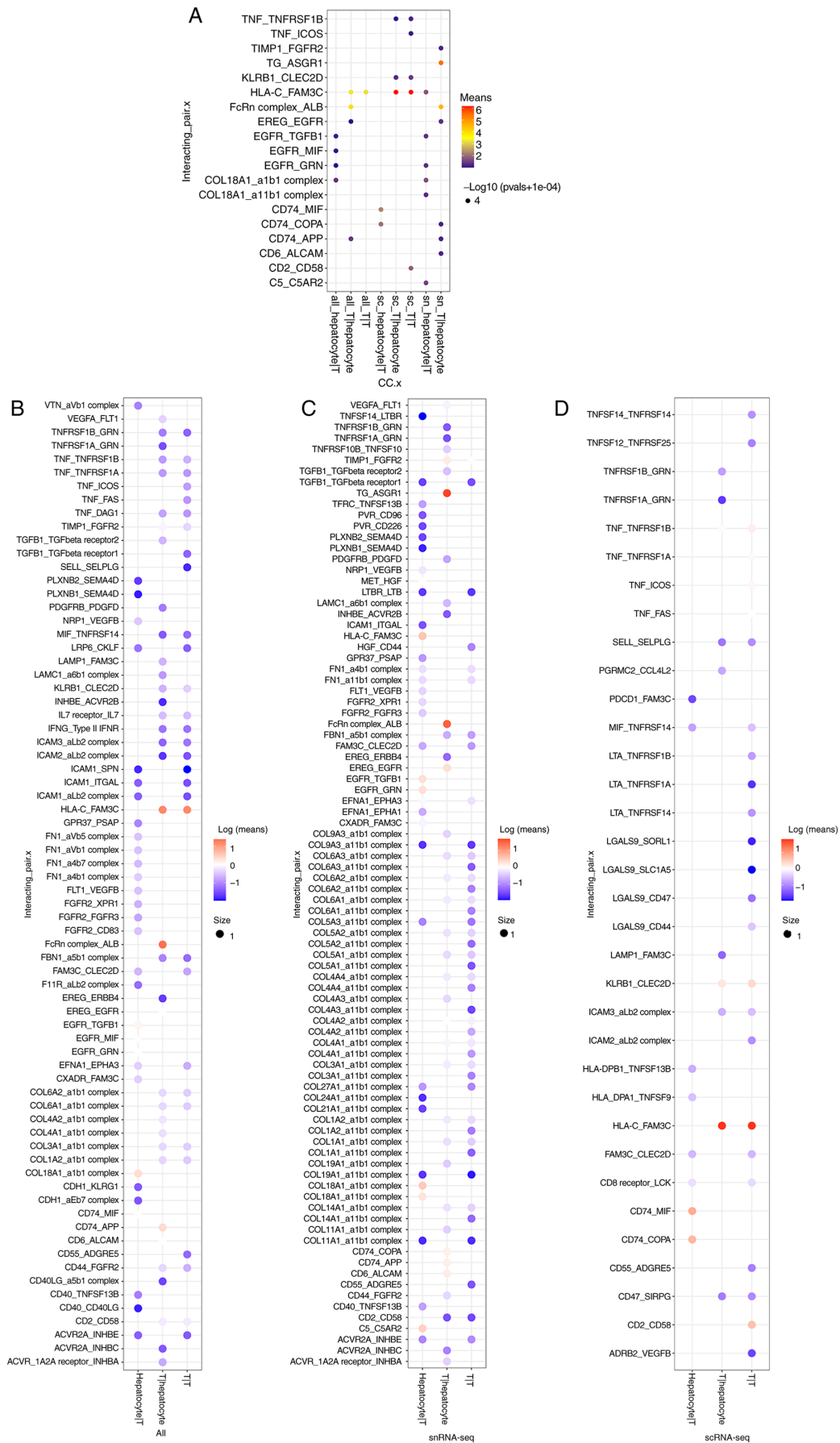


Figure 7. Interaction between hepatocytes and T cells. (A) Cell-cell interactions following further screening using mean >1. (B) Ligand-receptor interactions between hepatocytes and T cells (all, combined snRNA-seq with scRNA-seq). (C) Ligand-receptor interactions between hepatocytes and T cells (snRNA-seq only). (D) Ligand-receptor interactions between hepatocytes and T cells (scRNA-seq only). snRNA-seq, single-nucleus RNA sequencing; scRNA-seq, single-cell RNA sequencing.

identified a similar number of 'ligand-receptor interactions' between hepatocytes and T cells during the combined analysis, (Fig. 7B-D) which may be associated with the low number of hepatocytes covered by scRNA-seq.

Moreover, the results displayed in Fig. 7A demonstrate the interactions following further screening with a mean >1. Results of the present study demonstrated that T-T interaction was not detected using snRNA-seq (mean >1). Although snRNA-seq enriched a higher number of interactions, results obtained from the scRNA-seq may be more reliable.

Discussion

ScRNA-seq provides an advanced approach to the study of tumor cell heterogeneity and microenvironment. In the present study, the application of scRNA-seq and snRNA-seq methods in HCC were analyzed, providing a novel reference for understanding the application scope and selection of different sequencing methods.

Cells identified using snRNA-seq were mainly hepatocytes and fibroblasts, while the cells identified using scRNA-seq were mainly immune cells. This difference may result from the depletion of hepatocytes during the sorting phase of scRNA-seq, while immune cells are free and less likely to be subject to depletion. This result is also associated with the difference in sample processing (12). In the dissociation process of single-cell sequencing samples, different cell types exhibit different dissociation efficiencies (23,24). Compared with immune cells, epithelial cells are more embedded in the extracellular matrix, so they are more difficult to decompose.

Results of the present study demonstrated that scRNA-seq identified a low number of hepatocytes, which differed to the results obtained from previous studies (25,26). This may be due to HCC exhibiting a large organizational heterogeneity (27). Certain HCC tissues contain a high number of HCC cells, while others contain an increased number of non-parenchymal cells, such as fibroblasts (27,28). HCC develops from hepatitis B cirrhosis, when liver tissue contains a lot of fiber and the number of liver cells is reduced (29). Moreover, cirrhosis makes tissue digestion difficult and time-consuming; thus, liver cell activity decreases. On this basis, cell screening conditions (mitochondrial ratio <20%) caused more liver cell information to be deleted. In addition, in western countries, HCC is often due to alcoholic liver disease or non-alcoholic fatty liver disease (30), which differs from hepatitis B-related HCC. Therefore, the number of hepatocytes identified by scRNA-seq will differ. This further indicates that snRNA-seq may produce improved results for HCC associated with hepatitis B cirrhosis than scRNA-seq.

Epithelial cells in HCC tissue possess a high heterogeneity, which is an important factor affecting the course of disease and the corresponding therapeutic effects. Results of the present snRNA-seq analysis revealed that there are numerous different cell types in the tumor epithelium in HCC, which may play different roles in the progression of HCC. However, results obtained from the scRNA-seq analysis consisted of only a small number of cells in a subpopulation. These results suggested that nuclear sequencing exhibits an improved application value in the study of tumor epithelial heterogeneity.

A large number of diverse immune cells, including T cells, macrophages/monocytes, B cells and NK cells, were identified using scRNA-seq. The T cell population included different

subgroups: Naïve CD4⁺ T cells, effector CD8⁺ T cells and depleted CD8⁺ T cells. Notably, similar results were obtained during kidney studies (10). These results suggested that scRNA-seq exhibits an improved application value compared with snRNA-seq in the study of the tumor immune microenvironment.

The present study aimed to compare the differences between scRNA-seq and snRNA-seq methods in liver tissue, which may provide a novel theoretical basis for the selection of sequencing methods. In conclusion, the two sequencing methods may be used in combination to include both immune and epithelial cells.

Acknowledgements

Not applicable.

Funding

The present study was supported by the Qingdao Outstanding Health Professional Development Fund.

Availability of data and materials

The datasets used and analyzed during the current study are available from the GEO database (accession no. GSE210679).

Authors' contributions

HXQ and LX designed the experiments. FW and XJT performed the experiments and sample collection. FW conducted the bioinformatics analysis. HXQ, LX and FW confirm the authenticity of all the data. FW drafted the work manuscript. HXQ, LX and XJT revised the manuscript critically for important intellectual content. All authors read and approved the final manuscript.

Ethics approval and consent to participate

The present study was approved (approval no. 2021016) by the Ethics Committee of Qingdao Municipal Hospital (Qingdao, China). Informed consent was obtained from the patient.

Patient consent for publication

Informed consent was obtained from the patient.

Competing interests

The authors declare that they have no competing interests.

References

1. Slyper M, Porter CBM, Ashenberg O, Waldman J, Drokhlyansky E, Wakiro I, Smillie C, Smith-Rosario G, Wu J, Dionne D, *et al*: A single-cell and single-nucleus RNA-Seq toolbox for fresh and frozen human tumors. *Nat Med* 26: 792-802, 2020.
2. Xu L and Li C: Single-Cell transcriptome analysis reveals the M2 macrophages and exhausted T cells and intratumoral heterogeneity in triple-negative breast cancer. *Anticancer Agents Med Chem* 22: 294-312, 2022.
3. Wang Q, Wang Z, Zhang Z, Zhang W, Zhang M, Shen Z, Ye Y, Jiang K and Wang S: Landscape of cell heterogeneity and evolutionary trajectory in ulcerative colitis-associated colon cancer revealed by single-cell RNA sequencing. *Chin J Cancer Res* 33: 271-288, 2021.

4. Habib N, Avraham-Davidi I, Basu A, Burks T, Shekhar K, Hofree M, Choudhury SR, Aguet F, Gelfand E, Ardlie K, *et al*: Massively parallel single-nucleus RNA-seq with DroNc-seq. *Nat Methods* 14: 955-958, 2017.
5. Van Hauwaert EL, Gammelmark E, Sarvari AK, Larsen L, Nielsen R, Madsen JGS and Mandrup S: Isolation of nuclei from mouse white adipose tissues for single-nucleus genomics. *STAR Protoc* 2: 100612, 2021.
6. Basile G, Kahraman S, Dirice E, Pan H, Dreyfuss JM and Kulkarni RN: Using single-nucleus RNA-sequencing to interrogate transcriptomic profiles of archived human pancreatic islets. *Genome Med* 13: 128, 2021.
7. Fullard JF, Lee HC, Voloudakis G, Suo S, Javidfar B, Shao Z, Peter C, Zhang W, Jiang S, Corvelo A, *et al*: Single-nucleus transcriptome analysis of human brain immune response in patients with severe COVID-19. *Genome Med* 13: 118, 2021.
8. Maitra M, Nagy C, Chawla A, Wang YC, Nascimento C, Suderman M, Th  roux JF, Mechawar N, Ragoussis J and Turecki G: Extraction of nuclei from archived postmortem tissues for single-nucleus sequencing applications. *Nat Protoc* 16: 2788-2801, 2021.
9. Grindberg RV, Yee-Greenbaum JL, McConnell MJ, Novotny M, O'Shaughnessy AL, Lambert GM, Ara  zo-Bravo MJ, Lee J, Fishman M, Robbins GE, *et al*: RNA-sequencing from single nuclei. *Proc Natl Acad Sci USA* 110: 19802-19807, 2013.
10. Wu H, Kirita Y, Donnelly EL and Humphreys BD: Advantages of single-nucleus over single-cell RNA sequencing of adult kidney: Rare cell types and novel cell states revealed in fibrosis. *J Am Soc Nephrol* 30: 23-32, 2019.
11. Lake BB, Codeluppi S, Yung YC, Gao D, Chun J, Kharchenko PV, Linnarsson S and Zhang K: A comparative strategy for single-nucleus and single-cell transcriptomes confirms accuracy in predicted cell-type expression from nuclear RNA. *Sci Rep* 7: 6031, 2017.
12. Ding J, Adiconis X, Simmons SK, Kowalczyk MS, Hession CC, Marjanovic ND, Hughes TK, Wadsworth MH, Burks T, Nguyen LT, *et al*: Systematic comparison of single-cell and single-nucleus RNA-sequencing methods. *Nat Biotechnol* 38: 737-746, 2020.
13. Zeng W, Jiang S, Kong X, El-Ali N, Ball AR Jr, Ma CI, Hashimoto N, Yokomori K and Mortazavi A: Single-nucleus RNA-seq of differentiating human myoblasts reveals the extent of fate heterogeneity. *Nucleic Acids Res* 44: e158, 2016.
14. Thrupp N, Sala Frigerio C, Wolfs L, Skene NG, Fattorelli N, Poovathingal S, Fourn   Y, Matthews PM, Theys T, Mancuso R, *et al*: Single-nucleus RNA-Seq is not suitable for detection of microglial activation genes in humans. *Cell Rep* 32: 108189, 2020.
15. Morsey B, Niu M, Dyavar SR, Fletcher CV, Lamberty BG, Emanuel K, Fangmeier A and Fox HS: Cryopreservation of microglia enables single-cell RNA sequencing with minimal effects on disease-related gene expression patterns. *iScience* 24: 102357, 2021.
16. Yang JD, Hainaut P, Gores GJ, Amadou A, Plymoth A and Roberts LR: A global view of hepatocellular carcinoma: Trends, risk, prevention and management. *Nat Rev Gastroenterol Hepatol* 16: 589-604, 2019.
17. Global Burden of Disease Cancer Collaboration, Fitzmaurice C, Allen C, Barber RM, Barregard L, Bhutta ZA, Brenner H, Dicker DJ, Chimed-Orchir O, Dandona R, *et al*: Global, regional, and national cancer incidence, mortality, years of life lost, years lived with disability, and disability-adjusted life-years for 32 cancer groups, 1990 to 2015: A systematic analysis for the global burden of disease study. *JAMA Oncol* 3: 524-548, 2017.
18. Heinrich B, Gertz EM, Sch  ffer AA, Craig A, Ruf B, Subramanyam V, McVey JC, Diggs LP, Heinrich S, Rosato U, *et al*: The tumour microenvironment shapes innate lymphoid cells in patients with hepatocellular carcinoma. *Gut* 71: 1161-1175, 2022.
19. Payen VL, Lavergne A, Alevra Sarika N, Colonval M, Karim L, Deckers M, Najimi M, Coppieters W, Charloteaux B, Sokal EM and El Taghdouini A: Single-cell RNA sequencing of human liver reveals hepatic stellate cell heterogeneity. *JHEP Rep* 3: 100278, 2021.
20. Saviano A, Henderson NC and Baumert TF: Single-cell genomics and spatial transcriptomics: Discovery of novel cell states and cellular interactions in liver physiology and disease biology. *J Hepatol* 73: 1219-1230, 2020.
21. Qiu X, Mao Q, Tang Y, Wang L, Chawla R, Pliner HA and Trapnell C: Reversed graph embedding resolves complex single-cell trajectories. *Nat Methods* 14: 979-982, 2017.
22. Efranova M, Vento-Tormo M, Teichmann SA and Vento-Tormo R: CellPhoneDB: Inferring cell-cell communication from combined expression of multi-subunit ligand-receptor complexes. *Nat Protoc* 15: 1484-1506, 2020.
23. Uniken Venema WTC, Ramirez-Sanchez AD, Bigaeva E, Withoff S, Jonkers I, McIntyre RE, Ghouraba M, Raine T, Weersma RK, Franke L, *et al*: Gut mucosa dissociation protocols influence cell type proportions and single-cell gene expression levels. *Sci Rep* 12: 9897, 2022.
24. Burja B, Paul D, Tastanova A, Edalat SG, Gerber R, Houtman M, Elhai M, B  rki K, Staeger R, Restivo G, *et al*: An optimized tissue dissociation protocol for single-cell RNA sequencing analysis of fresh and cultured human skin biopsies. *Front Cell Dev Biol* 10: 872688, 2022.
25. Aizarani N, Saviano A, Sagar, Maily L, Durand S, Herman JS, Pessaux P, Baumert TF and Gr  n D: A human liver cell atlas reveals heterogeneity and epithelial progenitors. *Nature* 572: 199-204, 2019.
26. MacParland SA, Liu JC, Ma XZ, Innes BT, Bartczak AM, Gage BK, Manuel J, Khuu N, Echeverri J, Linares I, *et al*: Single cell RNA sequencing of human liver reveals distinct intrahepatic macrophage populations. *Nat Commun* 9: 4383, 2018.
27. Ng CKY, Dazert E, Boldanova T, Coto-Llerena M, Nuciforo S, Ercan C, Suslov A, Meier MA, Bock T, Schmidt A, *et al*: Integrative proteogenomic characterization of hepatocellular carcinoma across etiologies and stages. *Nat Commun* 13: 2436, 2022.
28. Heinrich S, Craig AJ, Ma L, Heinrich B, Greten TF and Wang XW: Understanding tumour cell heterogeneity and its implication for immunotherapy in liver cancer using single-cell analysis. *J Hepatol* 74: 700-715, 2021.
29. Deng R, Liu S, Shen S, Guo H and Sun J: Circulating hepatitis B virus RNA: From biology to clinical applications. *Hepatology*: Mar 28, 2022 (Epub ahead of print).
30. Shah PA, Patil R and Harrison SA: NAFLD-related hepatocellular carcinoma: The growing challenge. *Hepatology*: Apr 28, 2022 (Epub ahead of print).



This work is licensed under a Creative Commons Attribution-NonCommercial-NoDerivatives 4.0 International (CC BY-NC-ND 4.0) License.